Cladding-Mode-Resonances in Air–Silica Microstructure Optical Fibers

B. J. Eggleton, P. S. Westbrook, C. A. White, C. Kerbage, R. S. Windeler, and G. L. Burdge

***Abstract*—We present a comprehensive study of mode propagation in a range of different air–silica microstructured fibers. The inscription of both Bragg and long-period gratings (LPGs) into the photosensitive core region of microstructured air–silica fibers has allowed us to generate complex transmission spectra from a range of fibers with various fill fractions and with increasing air-clad hole diameters. The spectral characteristics for typical air-hole geometry's are explained qualitatively and modeled using beam propagation simulations, where the numerical modeling corroborates the experimental measurements. Specifically, the data reveal the propagation of higher order leaky modes in fibers with periodically spaced air-holes, and relatively small air-fill fraction. And as the air-hole diameter increases, spectra show cladding modes defined solely by the inner air-clad region. We describe these measurements and corresponding simulations and discuss their implications for the understanding of such air-hole structures.**

***Index Terms*—Birefringence, fiber optics, modeling, optical fiber applications, optical fiber cladding, optical fiber devices, optical propagation, periodic structures, polarization.**

I. Introduction

RECENT excitement has been generated by the demonstration of air–silica microstructured (ASM) optical fibers [1]–[7]. These fibers, which have been known since the earliest days of silica light guide research [1], come in different flavors (e.g., *photonic crystal* fibers [2]–[5], *honey-comb* fibers [6] or *holey* fibers [7]), and are usually single material fibers that incorporate numerous air voids in the cladding that run along the length of the fiber. As a result of the large controllable index variations that can be obtained in these fibers they can possess unique characteristics that allow a wide range of guidance properties with different guidance mechanisms. Guidance can occur as a result of a photonic bandgap created by a carefully selected periodic array of air-holes in the cladding region [8]. In such fibers, light is confined to a region of low index in the center of the fiber and guidance occurs for a frequency range in which light cannot propagate in the periodic cladding [8]. Another general guidance regime, which we consider further in this paper, is characterized by total internal reflection at the silica core and air-cladding region [2], [7]. More generally, total-internal reflection is achieved by an effective average refractive index difference between a central high-index silica core region and the surrounding air-hole cladding region.

Manuscript received March 3, 2000; revised May 17, 2000.

B. J. Eggleton, P. S. Westbrook, C. A. White, C. Kerbage, and R. S. Windeler are with the Bell Laboratories, Lucent Technologies, Murray Hill, NJ 07974 USA (e-mail: egg@lucent.com).

G. L. Burdge is with the Laboratory for Physical Science, College Park, MD 20740 USA.

Publisher Item Identifier S 0733-8724(00)06484-7.

Fig. 1(a)–(d) show ASM fibers with different air-hole fractions and air-hole distributions spanning guidance regimes from effective volume guidance to simple total-internal reflection. Fig. 1(a) shows a fiber that incorporates periodically spaced air-holes in the cladding region, with a relatively small air-fill fraction, referred to in this paper as *crystal fibers* [2]. This name is chosen to reflect the fact that this fiber comprises an approximately periodic arrangement of air-holes in the cladding region but that light is guided simply due to total internal reflection and is unaffected by photonic bandgap effects. In this fiber, the small-scale microstructure, created by the array of air-holes, allows the spatial distribution [2], effective index of modes [9], [10] and dispersion [7], [11], [12] to be controlled by the air-fill ratio and the ratio of propagation wavelength to air-hole diameter. As the air-hole size is increased, "*air-clad*" fibers of varying inner cladding diameters result. Several examples are shown in Fig. 1(b)–(d). In these fibers, propagation of modes is defined by an inner cladding—that region between the core and the surrounding air-holes, and guidance requires only a single layer of air-holes. Such mode confinement allows for waveguide properties similar to that of a fiber with a diameter equal to the inner cladding, and also isolates the fiber modes from the external environment (e.g., exhibits insensitivity to external index) [9], [13]–[16]. As the air-holes approach the central core region, a "*high-delta microstructured* optical fiber," is achieved as shown in Fig. 1(d). As discussed further below, such a fiber has similar characteristics to a step index fiber with an index difference corresponding to the air–silica index difference, in effect the largest possible delta achievable in a silica fiber. The modes in such a fiber are tightly confined by the air-holes and show strong anomalous dispersion at visible wavelengths [17], [18].

To date, research has focused on understanding the guidance properties of fundamental modes localized in the core region, for example, bend loss, cutoff wavelength [2], mode field diameter [7], and dispersion [11], [12], [17], [18]. Several applications have been considered including, the use of such fibers for dispersion compensation in lightwave transmission systems [12], the demonstration of fibers with large effective area for reduced nonlinearity [19] and fibers that are single-mode over broad spectral ranges [2]. More recently, Ranka *et al.* [17], [18] demonstrated fibers with small effective area and zero group velocity dispersion in the visible for enhanced nonlinear effects.

At present, many of the lightwave applications of these fibers are limited by the inherent losses; the loss has been reported to be as low as 50 dB/km [6]. Another broader class of applications for ASM fibers, where losses are not detrimental, is in the design of optical components, such as grating-based filters [9],

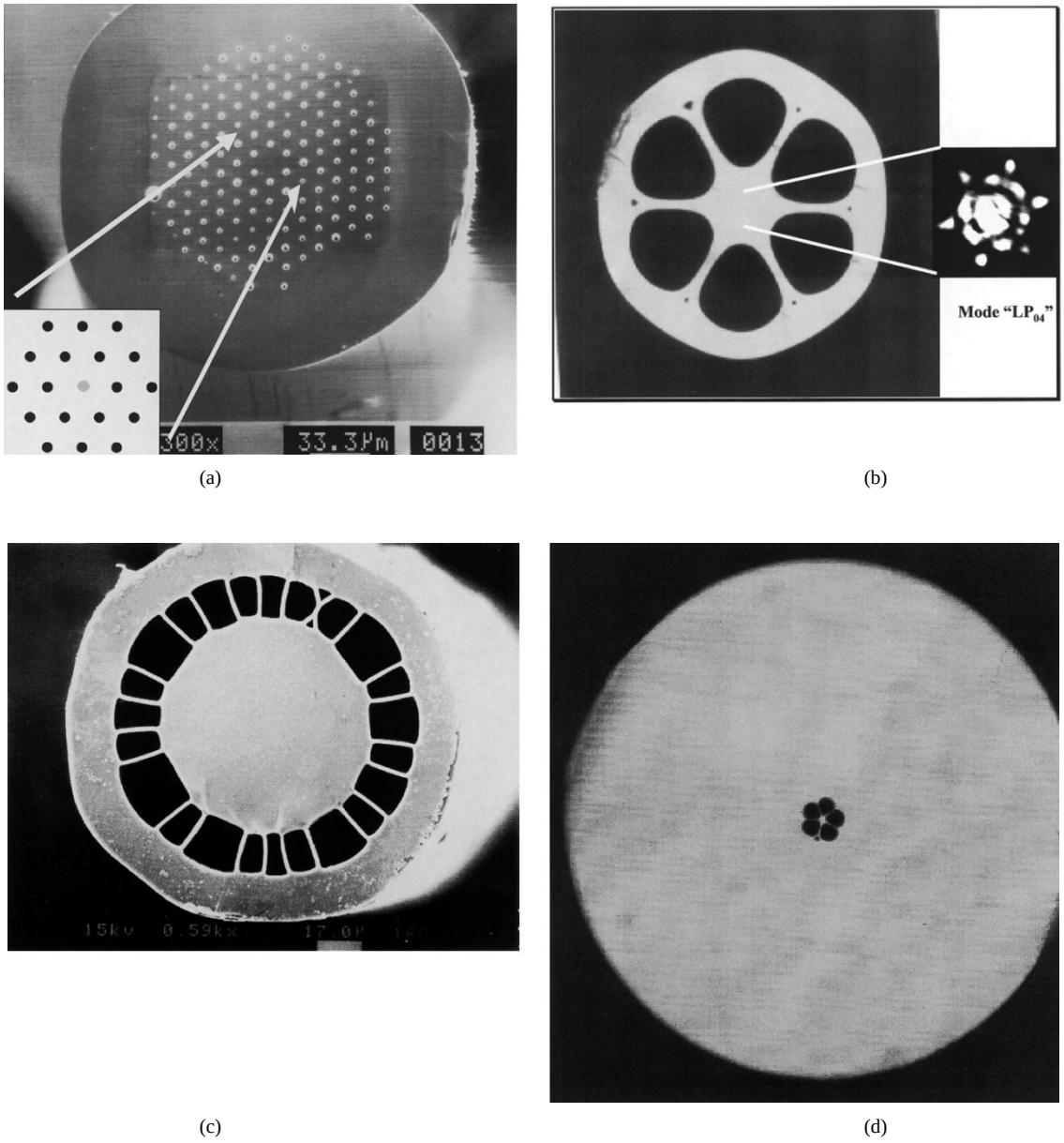

(a) (b)

(c) (d)

Fig. 1. SEMs and photographs of respective ASM optical fibers: (a) crystal fiber, (b) grapefruit fiber, (c) air-clad fiber, and (d) high delta microstructured optical fiber.

[10], [13]–[16]. In these applications, the air regions are not necessarily involved in core mode guidance, and are designed to manipulate higher order modes that propagate predominantly in the cladding region, referred to as *cladding modes.* In such fibers, core mode guidance is achieved simply by changing the composition of the core (e.g., doping with germanium), which allows for the fabrication of photosensitive gratings. In this context, these fibers can also allow for the introduction of active materials into the air-hole regions yielding novel hybrid waveguide devices [14]–[16]. This is the motivation for establishing a clear understanding of the transmission spectra of these gratings and the relation of these spectra to the characteristics of these cladding modes. Several applications of gratings in air–silica and hybrid polymer–silica waveguides have been demonstrated, including widely tunable long-period grating (LPG) filters [15], [16] with on-fiber thin-film heaters [14], LPG resonances that are insensitive to external index [10], [13], and a novel method for suppressing cladding mode loss in fiber Bragg gratings (FBGs) [15], [16].

A study of the spectra of gratings in ASM optical fibers is valuable because it allows for a full characterization of both core and cladding modes. In particular, a Bragg grating written into the core of such a fiber facilitates phase matching to counter-propagating higher order modes. When excited, these counter-propagating modes manifest themselves as resonant loss in the corresponding transmission spectrum thus providing a modal spectrum of the waveguide, revealing effective indexes (propagation constants). This can also provide a simple method for obtaining mode-field patterns of higher order modes of the waveguide. The modal properties obtained can be applied more generally to the design of components and transmission fibers.

In an earlier paper, we reported the fabrication of both FBGs and LPGs in a fiber comprising a periodic array of air-holes in the cladding (crystal fiber) [9], [10]. The transmission spectrum

of the FBG provided detailed modal characteristics of the fiber. For example, this characterization demonstrated the propagation of higher order leaky modes and showed that the effective index of these modes as well as their spatial distribution is determined by the air-fill fraction and the ratio of propagation wavelength to air-hole diameter. The associated near field mode images agreed very well with those obtained using beam propagation method (BPM) simulations [9], [10].

Following our earlier report [9], [10], in this paper, we present a detailed modal characterization of a range of different ASM optical fibers with limiting characteristics (e.g., air-fill fraction, ratio of propagation wavelength to air-hole diameter and air-hole distribution). These fibers, shown in Fig. 1(a)–(d), each demonstrate an ability to manipulate core and cladding modes in different ways, by the placement and distribution of the air-holes. They incorporate a small photosensitive region in the central core allowing for the inscription of both FBG and LPGs. By inspection of the transmission spectrum of the FBG written into the core of these fibers, we obtain a "mapping" of the different modes of the fiber. In particular this characterization provides effective indexes, mode-field distributions and polarization properties for both fundamental and higher order modes that propagate in the cladding. The spectra of these gratings are analyzed and explained qualitatively. We also show that BPM numerical methods can be effectively used to compute modal field shapes and propagation constants of transverse spatial modes of ASM fibers and in particular can accurately describe "leaky mode" propagation in crystal fibers. And in the design of grating structure we obtain good agreement between calculated results and experimental results. We discuss the implications of these results in more detail for the design of grating based devices and more generally in the applications of ASM optical fibers.

The paper is structured as follows: In Section II we review cladding mode resonances in both FBGs and LPGs. We then provide a description of BPM for computation of waveguide properties and establish the relationship between the transmission spectrum of a FBG and the modal spectrum computed using BPM. In Section III, we describe the fabrication of gratings in ASM optical fibers and experimental apparatus used to obtain mode-field images of grating excited modes. In Sections IV–VI, we present detailed results on grating spectra and near-field mode distributions for the different ASM optical fibers. The transmission spectra are analyzed and compared to numerical simulations using BPM.

II. Background

A. Cladding Mode Resonances

The primary measurement we use to study gratings in ASM optical fibers is their transmission spectrum. Fig. 2 shows, a schematic illustrating grating induced coupling from a guided core mode to a cladding mode, and a typical transmission spectrum of an FBG written in conventional fiber, see [20]–[22] for an excellent review. The sharp resonant loss on the short wavelength side of the Bragg resonance is due to coupling to these

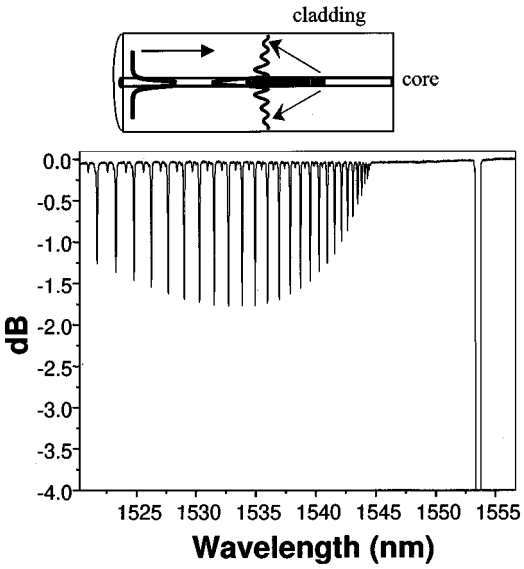

Fig. 2. Typical transmission spectrum of FBG exhibiting short wavelength loss. Each dip in the transmission spectrum is associated with grating facilitated phase matching to a counterpropagating cladding mode. The inset shows a schematic of Bragg grating in the core of a conventional optical fiber.

distinct cladding modes, which are confined by the glass–air interface. Since cladding modes have their optical power distributed throughout the cladding, the corresponding cladding mode spectrum is dependent on the structure of the cladding as well as the air–silica interface at the edge of the cladding. Cladding mode resonances are exploited in the design of FBG [22] and LPG [23] devices. In the case of FBG the cladding mode loss is often regarded as a nuisance where the short wavelength loss reduces the usable bandwidth (see for example Ref. [24]). In the case of LPGs these cladding modes are exploited in the design of band-rejection filters for flattening of optical amplifiers [23].

By examining the transmission spectrum of a FBG written into an ASM fiber, we expect to gain insight into the guidance properties of the core and cladding modes and to correlate these properties with images of the cladding mode field. In effect, the transmission spectrum provides a "mapping" of the waveguide modes that can be used to obtain effective indexes and mode-fields for the respective modes. For the relatively "weak" index gratings considered in this paper, the actual index modulation is only a weak perturbation on the modes of the waveguide. Thus we can examine the modes of the unperturbed guide using the grating by neglecting the relatively small effect of the grating on the modes, an approximation that is implicit in the use of coupled mode theory [25], [26].

The grating region is characterized by an index modulation, which may be nonuniform in the transverse dimensions x and y. The index variation is defined through the full expression for the index modulation in the core

$$\Delta n(x, y, z) = \Delta n(x, y) \cdot \cos(2\pi z/\Lambda_{\mathrm{FBG}}) \qquad (1)$$

where Λ_{FBG} is the period of the FBG. In this paper we assume the transverse index change to have circular symmetry. Consequently for fibers that exhibit symmetric cladding distributions we only observe coupling to symmetric modes.

A simple description of the core and higher order cladding modes can be obtained through direct inspection of the transmission spectrum of the FBG, and knowledge of the grating period $\Lambda_{\rm FBG}$. The effective index of the fundamental mode localized in the core region ($n_{co}^{\rm eff}$) can be determined using the Bragg condition $\lambda_B = 2n_{co}\Lambda_{\rm FBG}$; where throughout the following discussions we assume effective indexes. The effective indexes of the respective cladding modes can then be determined using the well known phase matching condition: $\beta_{\rm clad,\,i} + \beta_{01} = 2\pi/\Lambda_{\rm FBG}$ [26], where $\beta_{\rm clad,\,i}$ is the propagation constant of the ith cladding mode propagating in the opposite direction to the fundamental $\rm LP_{01}$ with propagation constant β_{01}. Rearranging the phase matching equation and using $\beta_{01} = (2\pi/\lambda)n$ it is straightforward to show that the effective index ($n_{\rm clad,\,i}$) of the ith cladding mode is given by,

$$n_{\rm clad,\,i} = \frac{\lambda_{\rm clad,\,i}}{\Lambda_{\rm FBG}} - n_{co} \tag{2}$$

where $\lambda_{\rm clad,\,i}$ is the wavelength for resonant coupling to the ith cladding mode. For wavelengths close to the Bragg resonance we can ignore the wavelength dependence of $n_{\rm core}$ and $n_{\rm clad}$.

The effective indexes obtained from inspection of the FBG spectrum can be used in the design of LPGs, which couple the fundamental core mode to copropagating cladding modes [23]. The phase matching condition for copropagating grating couplers [20], [21], [23] can be written as

$$\lambda_{{\rm LPG},\,i} = (n_{co} - n_{\rm clad,\,i})\Lambda_{\rm LPG} \tag{3}$$

where $\lambda_{{\rm LPG},\,i}$ is the resonant coupling wavelength and $\Lambda_{\rm LPG}$ is the period of the LPG. Neglecting dispersion, it is straightforward to show that the LPG resonance wavelength is proportional to the wavelength interval between the Bragg resonance and the cladding resonance in the FBG:

$$\frac{\lambda_{{\rm LPG},\,i}}{\Lambda_{\rm LPG}} = \frac{\Delta\lambda_i}{\Lambda_{\rm FBG}} \tag{4}$$

where $\Delta\lambda_i = \lambda_B - \lambda_{\rm clad,\,i}$ is the difference between the fundamental Bragg resonance (given by the Bragg condition) and the wavelength of the ith cladding mode resonance.

Predicting the peak intensities of the experimental grating spectra, however requires detailed knowledge of the modal distributions and use of coupled mode theory, which we explore below.

B. Coupled Mode Theory

The use of coupled mode theory for the treatment of fiber gratings has been well explored, see, for example, [20], [21]. For uniform FBGs (constant index modulation and grating period), which we consider in this paper, the transmission coefficient at the peak of the nth resonance is given by

$$T_i = 1 - \tanh^2(\kappa_i L) \tag{5}$$

where L is the length of the FBG [22] and κ_i is the coupling coefficient (given below) between the core and cladding mode i. The spectra consists of the contribution of each mode [given by equation (5)] at wavelengths determined by the modal composition, multiplied by a grating dependent shape factor.

The coupling constant κ_i of the ith cladding mode is proportional to an overlap integral of the core mode $(E_{\rm core}(x,\,y))$ with the cladding mode $(E_{\rm clad,\,i}(x,y))$ weighted by the transverse refractive index change in the grating region [20]–[22]

$$\kappa_i \equiv \left(\frac{\pi}{\lambda}\right) \int E_{\rm core}(x,\,y)E^*_{\rm clad,\,i}(x,\,y)\Delta n(x,\,y)\,dx\,dy. \tag{6}$$

The core and cladding mode E-fields are assumed to be normalized

$$\begin{aligned}\int & E_{\rm core}(x,\,y)E^*_{\rm core}(x,\,y)\,dx\,dy \\ &= \int E_{\rm clad,\,i}(x,\,y)E^*_{\rm clad,\,i}(x,\,y)\,dx\,dy \\ &= 1\end{aligned} \tag{7}$$

(6) highlights an important but obvious point: only modes that have spatial overlap with the grating region are excited via phase phase-matching. (7) ensures the coupling constants, κ_i, have the dimensions of length^{-1} and depend only on the spatial field distribution, and not the overall magnitude of the field. We further assume that the coupling between cladding modes $\kappa_{i,\,l}$ is small in comparison with the core-cladding coupling. This approximation is valid for conventional fiber where the grating index variation in the core represents a much smaller fraction of the cladding-mode field extent than of the core-mode field. This is less valid in some of the microstructured fibers considered in this paper. Nevertheless, we obtain good agreement between computed results and experimental spectra.

The determination of the coupling constants requires a modal decomposition of the core and cladding E-fields. Unfortunately, for ASM fibers, the direct computation of these modal fields is difficult using conventional mode solvers. This results from the relatively high contrast and sharp features between glass and air as well as the relatively high order and lossy nature of some of the cladding modes. We describe within the next section a method of computing these quantities with a simple extension of a well-known numerical scheme.

C. Beam Propagation Modeling Using Correlation Method

The beam-propagation correlation method provides a simple intuitive method of determining the modal spectrum and modal profiles for a waveguide [27]–[29]. It has been used extensively in the study of complex waveguides and is particularly well suited to computing mode evolution in waveguides that vary in the longitudinal direction and in geometry's where leaky modes are important. This latter point is of particular interest in this work where we consider the propagation of leaky cladding modes in different ASM fibers. Briefly, the BPM correlation method propagates a launched field profile within a waveguide. The correlation function of the initial profile with the propagated profile at each point (z) in the guide is constructed. The Fourier transformation of this correlation function extracts periodic variations, which determine the propagation constants for the modes of the system. To obtain accurate results using BPM, the launched profile must include the modes of interest,

and the propagation must be computed for a long enough distance to reliably separate the modes.

The determination of coupling coefficients using the BPM requires a deeper understanding of the details of the method. The propagation of the field along the z direction through a transverse guide can be written as

$$E(x, y, z) = \sum_i \alpha_i E_i(x, y) e^{-i\beta_i z} \tag{8}$$

where for each mode i, $E_i(x, y)$ is the transverse modal profile, α_i is the amplitude strength of each mode, and $\beta_i = 2\pi n_i/\lambda$ is the wavevector in the propagation direction z.

The BPM computes this function, $E(x, y, z)$, for all z given only the initial starting field $E(x, y, 0)$ and the refractive index profile of the guide. This propagation is accomplished without *a priori* knowledge of the modal decomposition, however; the propagation contains all the information about the modes [27]. Given $E(x, y, z)$ for many values of z, the correlation method then extracts α_i, β_i, and $E_i(x, y)$ for each of the modes which compose the launched initial profile.

The correlation method begins by computing a correlation function between the initial launched profile, and the profile at each z value

$$P(z) = \int E(x, y, 0) E^*(x, y, z)\, dx\, dy. \tag{9}$$

Since the mode profiles are orthogonal in the transverse plane, we can simplify $P(z)$ using the modal decomposition

$$P(z) = \sum_i \alpha_i \alpha_i^* e^{-i\beta_i z}. \tag{10}$$

The Fourier transform of $P(z)$ with respect to z will be sharply peaked at frequencies given by the propagation constants β_i; further, the relative intensities of these peaks will be given by the square of the strengths α_i of each mode. Since the α_i do not change with propagation, a mode not included in the launched profile will not be found by the BPM. By computing the Fourier transformation of $E(x, y, z)$ with respect to z

$$\begin{aligned} E(x, y, \beta) &= \int e^{-i\beta z} E(x, y, z)\, dz \\ &= \sum_i \alpha_i E_i(x, y) \delta(\beta - \beta_i) \end{aligned} \tag{11}$$

evaluated at β_i, we can uniquely determine the modal fields $E_i(x, y)$. As we show below, these fields compare well with the experimentally imaged modal fields. This step is often accomplished through a secondary BPM step, which directly evaluates the Fourier transform only at β_i.

Using these quantities $E_i(x, y)$ one could directly compute the coupling constants necessary for equation (6). However, this route requires multiple computational steps, including a quantitative determination of $E_i(x, y)$, which again is difficult for this type of microstructured fiber. An alternative method can use BPM with

$$E(x, y, 0) = \Delta n(x, y) E_{\text{core}}(x, y) \tag{12}$$

as the initial launched profile. Since the modes of the guide form a complete orthogonal set, we can decompose this launched profile into a combination of core and cladding modes just as in equation (8). Here, the strengths α_i within the launched profile are identical to the coupling constants (κ_i) necessary for a coupled mode analysiss

$$\alpha_i = \int E_i^*(x, y) \Delta n(x, y) E_{\text{core}}(x, y)\, dx\, dy \equiv \left(\frac{\lambda}{\pi}\right) \kappa_i. \tag{13}$$

Now by analogy with equation (10), the relative intensities of the Fourier transformed peaks determine the squares of the coupling coefficients. Thus we obtain the frequencies and coupling coefficients *without having to directly compute the modal fields.*

The BPM method makes several approximations, which should negligibly affect the computed grating spectra. These approximations include the use of a scalar wave equation, and the numerical effects inherent in BPM simulations, and the assumption that the grating does not strongly effect the modal properties of the guide. The use of a scalar wave equation has been well tested for understanding modal propagation [29]. Although significant difficulties may arise when attempting to compute polarization information for high contrast systems, the effective indexes, and modal profiles should and do compare well with our experimental measurements, which do not attempt to extract polarization or other vector quantities. However, we note that detailed quantitative comparisons for the high-delta microstructured optical fibers, discussed in Section VI, may require the use of a vector based computation method. The numerical issues concerning beam propagation on a finite grid have been well explored, and the results reported here are insensitive to changes in these numerical tolerances (grid size, propagation length, etc.). Finally, the assumption that the grating does not dramatically affect the modes of the guide can be assessed through a comparison of the computed and measured spectra, as well as a simple order of magnitude comparison between the relative changes in refractive index of the transverse and propagation directions.

III. Experiment

A. Fabrication of Gratings

Fabrication of FBGs in ASM optical fibers consisted of scanning a 242 nm beam along the length of a conventional phase mask [30], [31]. The ultraviolet beam was generated by an excimer-pumped, frequency-doubled dye laser, with a typical fluence of 500 mJ/cm^2/pulse. The grating fabrication in ASM optical fiber was not different from that in conventional fiber. Both the exposure level and dosage were typical for FBGs written in conventional fibers and no significant alignment problems were encountered. In the case of the crystal fiber, we observed significant scattering of the ultraviolet light from the air-holes during the writing. This resulted in a diffraction pattern in the far field beyond the fiber that was largely random. LPGs are similarly written using an amplitude mask and a ultraviolet beam which is scanned along its length [23]. A fluence of about 75 mJ/cm^2 at 40 pps was typically used from an unfocussed excimer laser at 248 nm.

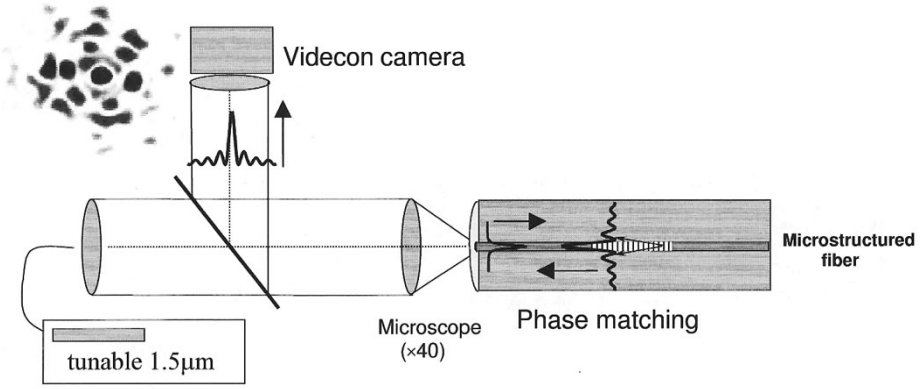

Fig. 3. Experimental setup used to characterize near field images for respective air–silica microstructured optical fibers. Bragg grating selectively excited counterpropagating "cladding modes" which are imaged in the near field on the VIDECON camera.

B. Modal Characterization

In order to fully characterize the waveguide properties of the various microstructured fibers, we performed systematic mode imaging. The experimental setup is shown in Fig. 3. A 1.55 μm tunable source was coupled into the reflective FBG using a beam-splitter. Light is coupled predominantly into the core mode. By tuning the wavelength of the source, we selectively excited different counter-propagating cladding modes, facilitated by phase matching provided by the FBGs. The light reflected off the FBG was imaged in the near field on a vidicon infrared (IR) camera using a microscope objective. Care was taken to keep the bare fiber straight and to avoid asymmetric stresses caused by clamping. A transmission spectrum of the FBG could then be obtained by measuring the power transmitted through the grating as the wavelength of the laser was tuned (resolution 3 pm). When capturing images of the reflected mode-field the far end of the fiber was placed in index-matching gel so as to minimize back reflections. For consistency, when describing these modes, we adopt the conventional nomenclature of referring to these higher order modes as "01," "02," etc., often associated with weak guidance.

IV. Crystal Fiber

The crystal fiber was first demonstrated by Russell and co-workers [3], [4], [19], [32] and consisted of an all-silica fiber with a periodic array of air-holes in the cladding, referred to as *photonic crystal fiber* by these authors. These authors suggested various applications of these fibers including large effective area for reduced nonlinearity [19], as well as describing fibers that were "endlessly" single mode [2]. This latter property was explained using an effective index model in which the cladding index is wavelength dependent; at short wavelengths light is more confined in the glass regions, avoiding the air holes and increasing the effective index of the cladding. The results presented below are consistent with this work and further explore the detailed nature of higher order modes that propagate in the cladding.

A. A Crystal Fiber Design

Fig. 4 shows a schematic of the crystal fiber [also in Fig. 1(a)]. The crystal fiber was designed with a sufficiently small photosensitive germanium core such that it would appear as a small perturbation on the guided modes of the fiber but contain sufficient germanium to write a grating. A typical crystal fiber has a core of photosensitive germanium with radius $\rho \sim 1$ μm, and $\Delta = (n_{\rm core} - n_{\rm clad})/n_{\rm core} \sim 0.5\%$, where $n_{\rm core}$ and $n_{\rm clad}$ are, respectively, the refractive index of the germanium core and the inner silica cladding, with a corresponding $V = 2\pi\rho/\lambda\sqrt{n_{\rm core}^2 - n_{\rm clad}^2} \sim 0.6$ at $\lambda = 1.55$ μm (ignoring the surrounding air-holes). The core is surrounded by a hexagonal array of holes in a silica matrix with an air hole diameter $d \sim 2$ μm and spacing $\Lambda \sim 10$ μm extending to a radius of $\sim$60 μm, corresponding to six to seven layers ($d/\Lambda \sim 0.2$ and $\Lambda/\lambda \sim 6.5$ at 1.5 μm). An outer silica region of 200 μm surrounded the lattice of air-holes. Note that this fiber, guides simply due to internal reflection and, with a lattice constant of 10 μm, is not expected to be influenced by photonic bandgap effects at these wavelengths.

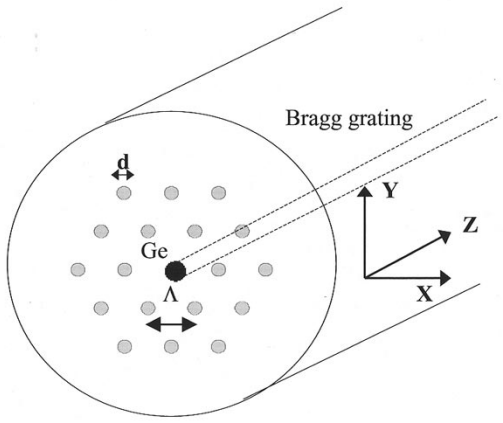

Fig. 4. Schematic of photosensitive crystal fiber showing air-holes and core regions. The pitch is $\Lambda = 10$ μm, hole diameter $d = 2$ μm. and germanium core radius $\rho = 1$ μm (seven layers of air-holes).

B. Crystal Fiber Grating Spectra

The fiber was deuterium loaded to enhance the photosensitivity of the germanium region and was exposed through a conventional phase mask with a period of $\Lambda_{\rm MASK} = 1.075$ μm ($\Lambda_{\rm FBG} = \Lambda_{\rm MASK}/2$) at a fluence of 240 mJ/cm^2/pulse. The ultraviolet exposure was a 4 cm, constant velocity scan of a 7

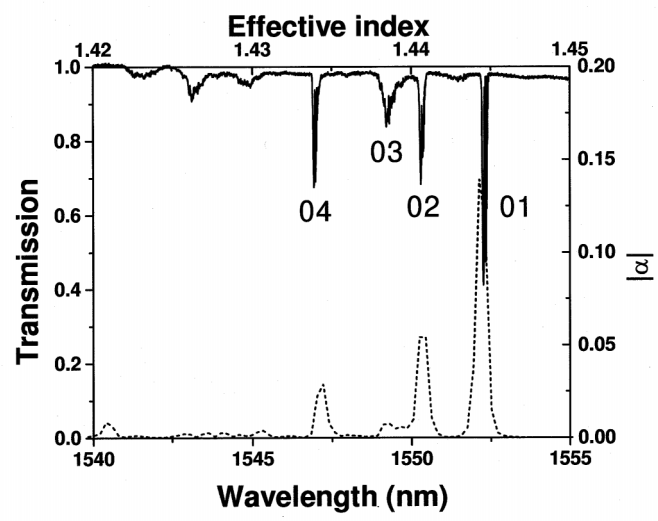

(a)

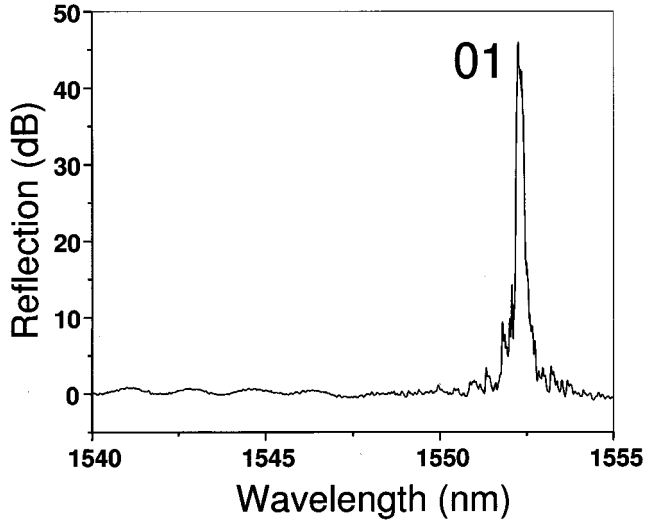

(b)

Fig. 5. (a) Measured (solid line) transmission spectrum of FBG written in crystal fiber before (solid line), calculated modal spectrum (dashed line) and measured spectrum (dotted line) after application of external index (difficult to see) and (b) measured reflection spectrum.

mm FWHM Gaussian beam for 1000 seconds, yielding a peak index modulation of $\Delta n \sim 4 \times 10^{-5}$. Because of the small germanium core, the overlap of the fundamental mode with the grating is substantially less than in a conventional fiber, where it is typically 80% [22]. We show below that the overlap between the core mode and the grating region in the crystal fiber is only $|\alpha_1| \sim 0.3$, giving $\kappa_1 = \pi \Delta n \alpha_1 / \lambda \sim 0.25\ \text{cm}^{-1}$ and $\kappa L \sim 1$. The increase in the effective index of this mode, due to the ultraviolet exposure, is only $\Delta n_{\text{UV}}^{\text{eff}} \sim 10^{-5}$ and is thus a small perturbation on the actual modal properties of the fiber.

The solid line in Fig. 5(a) shows the transmission spectrum of the FBG; the top axis shows the computed effective index using (2). It was measured after the grating was suitably annealed to remove deuterium. The dashed line shows the computed modal spectrum, described below, where the right vertical axis is the mode overlap defined in equation (13). Fig. 5(b) shows the measured reflection spectrum obtained by splicing the crystal fiber directly onto standard fiber using a three-port circulator. Note only one resonance appears ("01") in the reflection spectrum. As we show below, the other resonances in transmission spectrum Fig. 5(a) correspond to higher order leaky modes that are quickly dissipated upon propagation. They are analogous to cladding mode resonances of a conventional FBG [20], see Fig. 2. Resonance labeled "01" therefore corresponds to reflection of the core guided mode and indicates that the fiber is single-mode at 1.55 μm. This observation is consistent with the analysis of Russell *et al.* [2].

Using the Bragg condition we estimate the effective index of the fundamental mode ("01") to be $n_{co}^{\text{eff}} = 1.444$, which is essentially that of silica at $\lambda = 1.5$ μm. We note that this observation implies that the fundamental mode is only very weakly guided by the crystal fiber, a result that is confirmed by the high bend sensitivity. Furthermore, we note that in a similar fiber without a raised central index region (e.g., Ge core), such as those described by Russell and coworkers [2], the core mode would have an effective index slightly below that of silica and thus would be leaky, ultimately absorbed by the polymer jacket.

The effective index of other modes can be determined using the phase matching condition (3). These results are summarized in Table I, along with results from numerical simulations using BPM simulations, described further below. Several qualitative statements can be made about the highly irregular transmission spectrum of the FBG written in crystal fiber. First, the cladding mode resonances have similar coupling strengths compared to the fundamental resonance. As we show below, cladding modes of this fiber are confined by the lattice of air-holes; in effect the array of air-holes forms an effective inner cladding. Consequently, these first few cladding modes have relatively large overlap with the grating region, compared to a similar strength grating in conventional fiber. Second, the spacing of respective cladding mode resonances is larger than in a conventional fiber (cf., Fig. 2), also because of the reduced effective cladding diameter. Finally, the onset of cladding mode loss is determined by the core/cladding effective index difference (Δn_{eff}) [24]. In the case of the crystal fiber, the effective index difference of the cladding is not well defined and is strongly wavelength dependent [2]. Nevertheless, one can obtain an estimate of Δn_{eff} by careful examination of Fig. 5(a) (and other similar spectra not shown here). The onset of loss at $\sim$1551.53 nm gives $\Delta n_{\text{crystalfiber}}^{\text{eff}} \sim 1.3 \times 10^{-3}$ (corresponding to $\Delta \sim 0.1\%$), which within experimental uncertainty, is consistent both with the analysis of [32] and with the fiber being single mode.

We subsequently wrote an LPG in the crystal fiber. Using the results summarized in Table I and (3) and (4) we estimate a grating period of $\Lambda_{\text{LPG}} = 155$ μm for a LPG coupling into resonance "04" [Fig. 5(a)] at $\lambda_n \sim 1.55$ μm. Upon annealing the exposed fiber, we recorded the transmission spectrum shown in Fig. 6 (solid line), with a resonance at $\sim$1.6 μm; where the shift may be attributed to some uncertainty in determining the effective indexes of the respective modes and annealing. A second strong resonance was also observed at $\sim$1050 nm. We note two observations concerning this resonance: 1) the temperature dependence was measured to be $\sim$0.02 nm/C and 2) the polarization splitting was $\sim$0.1 nm. Both of these are relatively low for a LPG.

TABLE I
SUMMARY OF EFFECTIVE INDICES OF RESPECTIVE MODES OF CRYSTAL FIBER

Mode label	λ_n(nm)	Re{n_{eff}} exp.	Re{n_{eff}} BPM.
01	1552.29	1.4439	1.4442
02	1550.29	1.4402	1.4404
03	1549.19	1.4382	1.4385
04	1546.99	1.4341	1.4342

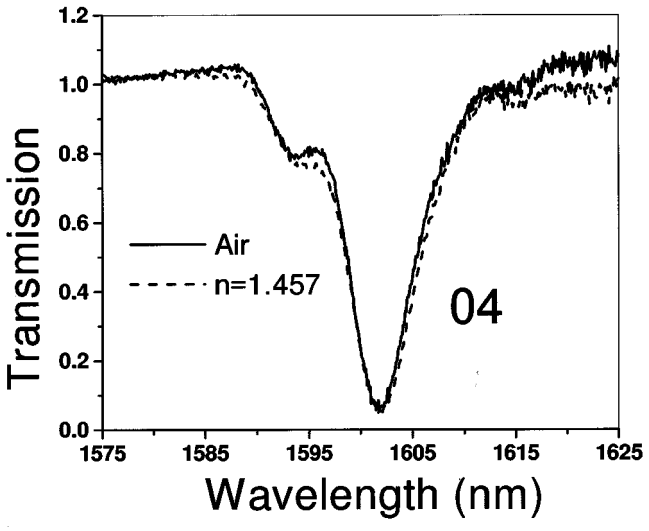

Fig. 6. Measured transmission spectrum of LPG written in crystal fiber before (solid line) and after (dashed line) application of external index.

Both the FBG and LPG were then immersed in index matching liquid with an index of $n = 1.457$ (at 632.8nm). The dotted lines in Figs. 5(a) and 6 show, respectively the transmission spectrum of the FBG and LPG after application of the external index. Note that there is no noticeable change in the spectrum. In fact the dotted line cannot clearly be resolved in this figure as the transmission spectra is completely unchanged. In particular, the insensitivity of the FBG spectrum to external index indicates that these cladding mode resonances are confined by the array of air-holes, that is, there is negligible power at the glass/air interface. This result is in contrast with conventional gratings whose cladding mode spectra are dramatically affected by changes in the external index, see for example Ref. [13], [20].

C. Crystal Fiber Cladding Modes

In order to better understand the propagation of the cladding modes of the crystal fiber, we performed a series of cutback measurements. The fiber was cleaved several times at several different lengths between the FBG and the observation plane to allow for different propagation lengths of the reflected modes. These experiments revealed that, whereas mode "01" had relatively low loss, modes "03" and "04" only propagated several centimeters beyond the grating. Mode imaging measurements were then performed on the remaining fiber, using a $\times 40$ objective (see Fig. 3). Fig. 7(a) and (b) shows, respectively, near field images when the laser wavelength is tuned to: a) 1549.196 nm resonance "03" and b) 1546.990 nm resonance "04." Note that the shape of the mode field images reflect the hexagonal symmetry of the lattice and that much of the energy is confined to the inner few rings or holes. Note that the apparent "hole" in the center of the mode is an artifact of the numerical simulation plotting routine.

Numerical simulations using BPM were then performed. The BPM simulation [29], [33] consisted of exciting the crystal fiber (Germanium core and 7 layers of air-holes in a hexagonal array, surrounded by infinite silica cladding) with a symmetric on-axis Gaussian beam with a beam waist of $2\ \mu$m, corresponding approximately to the width of grating region (see Section II-C). No z-dependence was included in this simulation and the ultraviolet-induced index change is only a weak perturbation on the waveguide modes. The correlation method computed the modal spectrum, mode eigenfunctions and corresponding effective indexes [27].

The dashed line in Fig. 5(a) shows the calculated modal spectrum, which qualitatively resembles the transmission spectra shown by the solid line in Fig. 5(a) [see (13)]. These simulations showed that modes 02 and higher are leaky, that is, their propagation constants are complex [34]. The real part of the effective indexes of the modes closely matched those of measured resonances (see Table I) and show "even" mode intensity patterns, see Fig. 7, that are similar to our observations ("02" and "04"). These simulations confirm that the effective indexes of these modes, as well as the spatial distribution of cladding modes, and thus associated grating spectra, are determined by the crystal fiber design, including, in particular, the air-fill fraction and ratio of propagation wavelength to air-hole diameter. The calculated imaginary part of the modes yields a similar loss length to that determined from the cutback measurements ($\sim$1–2 dB/cm), and indicates that any imperfections in lattice only play a small role in making the cladding mode resonances of the crystal fiber lossy. We may conclude that cladding modes of this crystal fiber, which have effective indexes below that of silica, are stripped off by the high index outer silica region and that there is negligible coherent feedback from the outer silica air interface. We note that similar leaky cladding modes have been observed in depressed-cladding fibers [35], [36] and fibers surrounded with high index polymers [34].

V. AIR-CLAD FIBER

As the air-hole diameter increases, such as when a crystal fiber geometry transitions to an air-clad fiber geometry, the

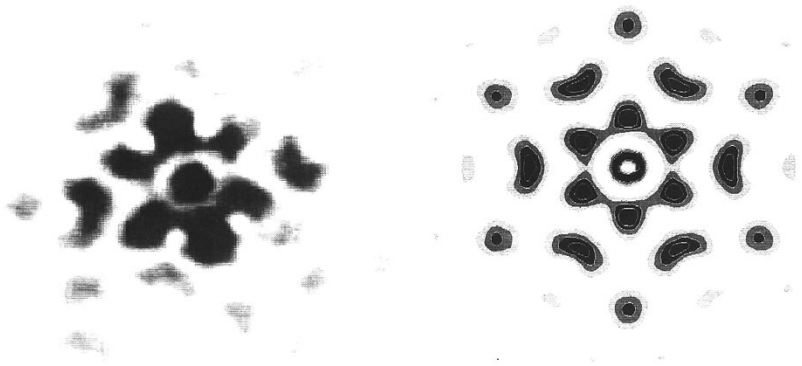

(a)—03

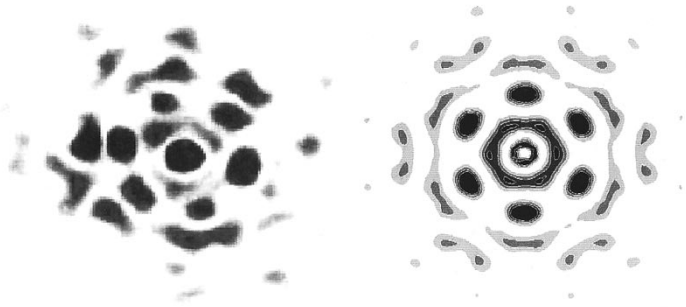

(b)—04

Fig. 7. Near field images light reflected off FBG when the tunable laser wavelength is tuned to: (a) 1549.196 nm, corresponding to the resonance labeled "03". (b) 1546.990 nm corresponding to the resonance labeled "04." The second column shows corresponding numerically simulated mode profiles.

modal properties are expected to change dramatically. In this limit the cladding modes are defined solely by the inner air-clad region and not by the outer cladding. These fibers also allow for the introduction of polymers into the air-hole regions yielding novel hybrid air–silica polymer waveguides.

A. Grapefruit Fiber Design

Fig. 8 shows a schematic of the "grapefruit" ASM fiber [also see Fig. 1(b)]. The physical and optical properties of this fiber differ significantly from the crystal fiber. It incorporates six large air-holes that form an approximately 40 μm air annulus around a central silica region 32 μm in diameter, with a corresponding air-fill fraction of $\sim$30%. The center of this region contains a germanium-doped core of diameter ~ 8 μm and $\Delta \sim 0.35\%$. The core mode is confined to the central region of the fiber and is mostly unaffected by the air-hole regions.

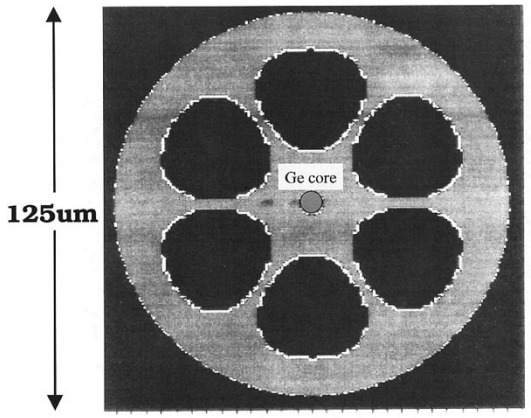

Fig. 8. Shows a cross section of the 130 μm diameter grapefruit fiber with its ~ 40 μm diameter air hole.

B. Grapefruit Fiber Grating Spectra

This fiber was deuterium-loaded, and an apodized FBG with period $\Lambda_{\rm FBG} = 0.538$ μm, length 4 cm, and $\Delta n \sim 0.0002$ was ultraviolet written into the fiber core. The solid line in Fig. 9 shows part of the transmission spectrum of the FBG. Note that the cladding loss spectrum is modified from that in a standard silica cladding fiber (see Fig. 2) by the unusual air–silica geometry. In particular, the wavelength spacing is larger than the lowest order cladding resonances in conventional fiber. As we show below, these resonances correspond to the few cladding modes that are confined primarily in the small diameter silica region and thus have large overlap with the core mode. Little light from these low order modes leaks out of the webbing between the holes, so the outer silica region has almost no influence on the mode structure for the inner cladding modes. The wavelength spacing of these cladding modes is larger than the lowest order cladding resonances in conventional fiber, because the spacing between the mth and $(m+1)$th resonance varies approximately as the inverse of the square of the waveguide diameter: $\Delta\lambda_m \sim (1+2m)/D_{\rm clad}^2$, where $D_{\rm clad}$ is the diameter of the inner cladding.

The remainder of the cladding mode spectrum consists of smaller resonances whose mode field patterns are distributed throughout the waveguide. This effect is demonstrated in Fig. 10

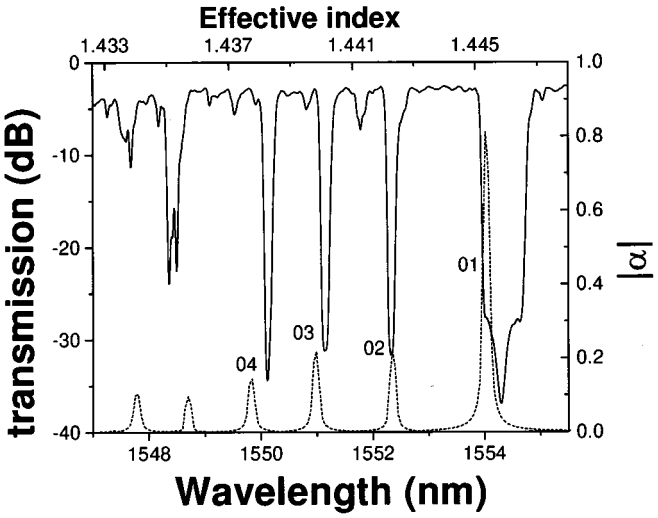

Fig. 9. Part of transmission spectrum of FBG written into the core of the grapefruit fiber (solid line) and calculated modal spectrum of the grapefruit fiber (dashed line).

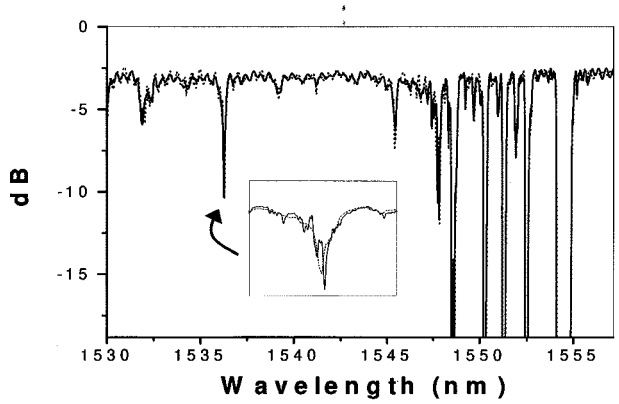

Fig. 10. Transmission spectra of FBG written into the core of the grapefruit fiber before (solid line) and after (dashed line) application of external index matched fluid. The inset shows a higher order cladding mode resonance being slightly perturbed by surrounding the fiber with index matched fluid.

by the dashed line for a FBG written in such a fiber that has been immersed in index matching oil ($n = 1.457$ @ 632 nm). The low order modes in the two cases are identical. As can be seen in the left resonances of Fig. 10, and the inset, the higher order modes, which interact with the external cladding-oil interface, are slightly affected. The fact that they are only slightly perturbed illustrates that these higher order modes are confined by both the inner and outer cladding.

C. Grapefruit Fiber Cladding Modes

Mode imaging measurements were then performed using the FBG in reflection. Fig. 11 show near field mode images obtained when the laser wavelength was tuned to

a) 1553.96 nm (the LP_{01} mode);
b) 1552.39 nm (LP_{02});
c) 1550.84 nm (LP_{03});
d) 1549.73 nm (LP_{04});
e) 1547.36 nm (LP_{05}).

Note that these mode shapes reflect the hexagonal symmetry of the grapefruit fiber and that for the lower modes (LP_{01}–LP_{04}) much of the energy is confined to the inner cladding region. These lower order cladding modes exhibit low loss and have relatively low bend loss, in contrast to the crystal fiber. Fig. 11(f) shows a higher order cladding mode, when the laser was tuned to 1535.82 nm. Fig. 11(g) shows a larger view of the same cladding mode and illustrates that this higher order cladding mode has a small amount of energy in the outer cladding region. Indeed this cladding mode resonance exhibits a small sensitivity to external index as was shown in Fig. 10. The azimuthal variation in cladding index variation allows this higher order cladding mode and others not shown here to tunnel into the outer silica region.

The grapefruit fiber was modeled using BPM simulation. This simulation consisted of exciting the fiber, illustrated schematically in Fig. 8, (germanium core surrounded by six air-holes with cylindrical glass air-interface) with a symmetric on-axis Gaussian beam with a beam waist of 8 μm, corresponding approximately to the width of grating region. The dashed line in Fig. 9 shows the computed modal spectrum of the grapefruit fiber where the agreement between the measured spectrum and computed spectrum is good particularly for the lower order modes. The second column in Fig. 11 shows the corresponding numerically simulated mode profiles and the data is summarized in Table II.

D. Hybrid Air–Silica Polymer Waveguide

The small effective diameter of the grapefruit fiber can be exploited in the design of tunable LPG filters, which can be adjusted over a substantially larger bandwidth than similar LPG filters in conventional fiber [15], [16]. The enhanced tunability stems from two factors: the relatively large spacing of the lower order cladding modes (proportional to the inverse square of the cladding diameter) and the fact that air regions may be infused with a material such as a polymer whose refractive index relative to silica may be tuned (through temperature variation). If the polymer refractive index is below n_{silica}, total internal reflection will occur at the boundary, resulting in a phase shift that depends on the tunable polymer–silica index difference. The resulting cladding mode resonance condition, (and hence LPG resonance wavelength) will be tunable. The degree of tunability of a given resonance is determined by the spacing of the cladding mode resonances, since, roughly speaking, each resonance corresponds to another factor of π accumulated phase shift, and the phase shift upon total internal reflection may be varied between 0 and $\pi/2$ by changing the index difference. Thus, the tuning range (or slope of the wavelength shift versus polymer–silica refractive index difference) is proportional to cladding resonance spacing [15], [16], [37]. Hence, by incorporating materials into the air-hole regions tunable LPGs can be realized with tuning bandwidths larger than can be achieved in conventional fibers with pure silica claddings.

In one such experiment an acrylate-based polymer with index close to that of silica was introduced into the air regions of the grapefruit fiber. The polymer was then UV cured to form a hybrid waveguide at the grating, as illustrated in Fig. 12. Heating the fiber changed the index of the polymer and tuned the resonance wavelength of a grating [see (3)].

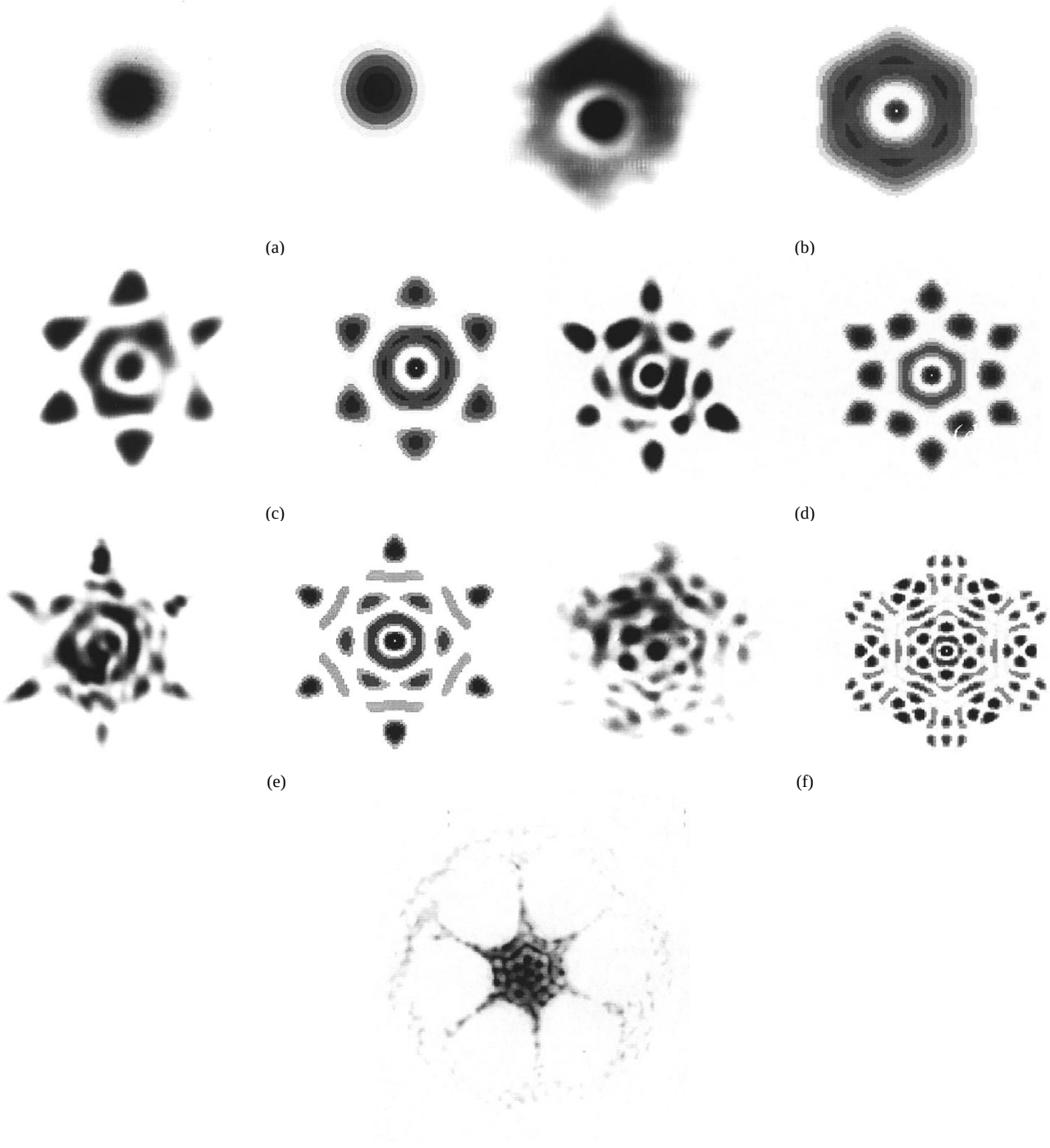

Fig. 11. Near-field images of light reflected off FBG when the laser was tuned to: (a) (01) 1553.96 nm (the LP_{01} mode); (b) (02) 1552.39 nm (LP_{02}); (c) (03) 1550.84 nm (LP_{03}) mode; (d) (04) 1547.82 nm (LP_{04} mode); (e) (05) 1547.36 nm (LP_{05} mode); (f) (06) 1535.82 nm; (g) a larger view of cladding mode (f). The second column shows corresponding numerically simulated mode profiles.

Using the effective indexes obtained from inspection of the FBG transmission spectra and the phase matching condition for an LPG, a period of $\Lambda_{\mathrm{LPG}} = 550\ \mu$m was chosen to couple into cladding mode resonance LP_{02} of Fig. 9(a). The polymer used in this experiment had an index that was slightly below that of silica and so the corresponding mode spatial distribution is similar to that in Fig. 11(b). The high optical losses of the polymer frustrate propagation through the polymer filled regions and thus the mode effectively sees an infinite lossy cladding and is completely unaffected by the external cladding. The outer air–silica interface remains in tact, allowing, for example, on-fiber thin film heaters for temperature tuning [14], [38]–[40].

The temperature dependence of the resulting cladding mode resonance is shown in Fig. 13. The tuning range is in excess of 150 nm for this LPG, which is significantly larger than could be

TABLE II
SUMMARY OF EFFECTIVE INDEXES OF RESPECTIVE MODES OF GRAPEFRUIT FIBER

Mode Label	λ_n (nm)	n_{eff} exp.	n_{eff} BPM
01	1553.96	1.4455	1.4455
02	1552.39	1.4425	1.4422
03	1550.84	1.4396	1.4398
04	1549.73	1.4341	1.4379
05	1547.36	1.4331	1.4346

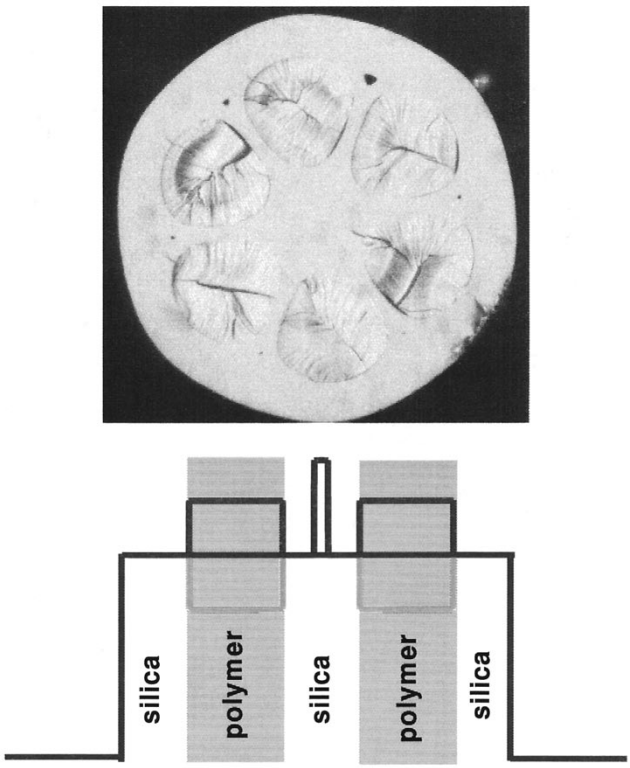

Fig. 12. (a) Photo of hybrid polymer air–silica microstructured optical fiber and (b) schematic.

obtained in a conventional fiber [34], [37], [41]. These results show that this tunability may be achieved through temperature control with an integrated, robust geometry in ASMs and illustrates the potential for enhancing the tunability, due to the small effective cladding diameter.

E. Air-Ring Fiber

We studied a second type of air-clad fiber shown in Figs. 14(a) and 1(c). This air-ring fiber resembles conventional fiber with a standard core and an inner cladding region, but a ring consisting mostly of air, surrounds the inner cladding [13], [14], [39], [42]. This "air-cladding" is protected by an outer silica tube, which is held in place by thin silica webs. This fiber has been used in recent demonstrations of external index-insensitive, LPGs [13] and electrically-tunable LPGs [14]. Fig. 14(b) shows the transmission spectrum of a FBG written in this fiber,

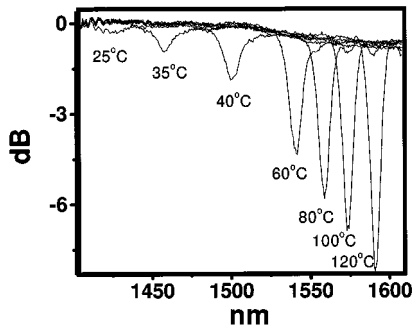

Fig. 13. Spectrum of LPG in hybrid polymer–silica fiber at different temperatures.

i.e., closely spaced cladding mode resonances much weaker in strength than the Bragg resonance. Indeed this transmission spectrum resembles that of a grating written in conventional fiber, as illustrated in Fig. 2. Fig. 15 show near field mode images obtained when the laser wavelength was tuned to: a) 1539.30 nm (the LP_{02} mode); 1539.20 (LP_{03}); and 1539.00 (LP_{04}). These modes closely resemble those of conventional optical fibers, LP_{02}, LP_{03}, LP_{04}, and are only slightly perturbed by the silica webbing.

VI. HIGH-DELTA MICROSTRUCTURED OPTICAL FIBER

As the air-holes approach the core region their influence on the core mode increases. As discussed further below, such a fiber has similar characteristics to a step index fiber with an index difference corresponding to the air–silica index difference, in effect the largest possible delta achievable in a silica fiber. This geometry provides strong anomalous dispersion at visible wavelengths as well as reduced effective area [17], [18]. The unusual modal properties of this fiber are explored below by inscribing an FBG in the core of the fiber. In particular the spectra show dramatically reduced cladding mode loss due the large spacing of lower order cladding modes and strong birefringence.

A. High-Delta Fiber Design

Fig. 16(a) and (b) shows respectively, a photo of the central region of the high-delta microstructured fiber, as well as a schematic. This high-delta microstructured optical fiber had a photosensitive germanium core of radius ~ 1 μm and $\Delta = (n_{co} - n_{\text{clad}})/n_{\text{core}} \sim 0.5\%$, where n_{co} and n_{clad} are the refractive index of the germanium core and the inner silica cladding,

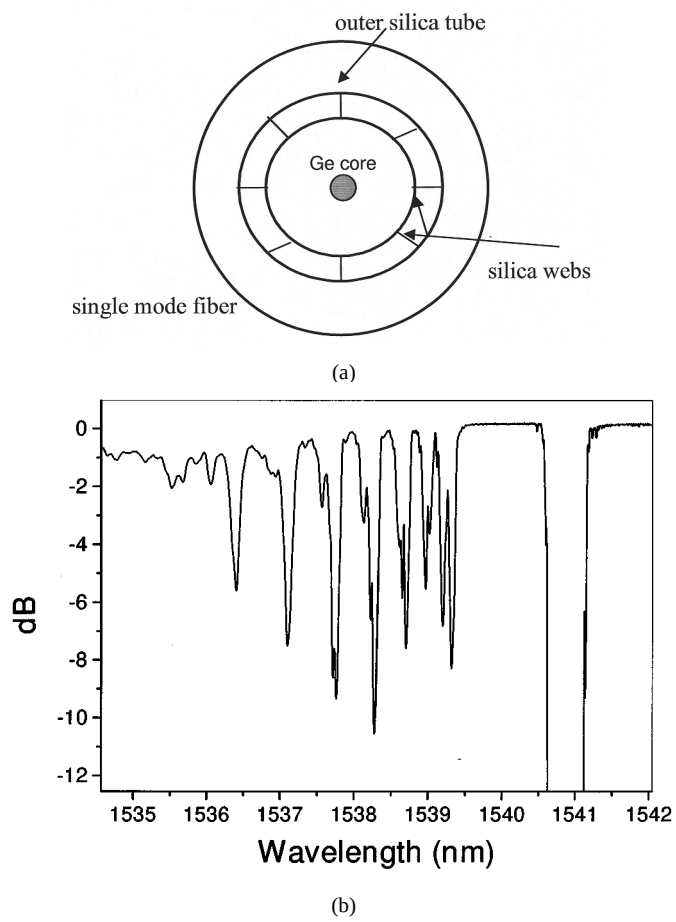

Fig. 14. (a) Schematic of the air-ring fiber and (b) transmission spectra of FBG written into the core of the air-ring fiber.

respectively. Approximately 2 μm from the center of the germanium core are five air-holes approximately 7 μm in diameter. The outer silica cladding extends to a diameter of 175 μm. Note also the small interstitial air-hole with diameter <0.5 μm. This fiber represents an extreme case of the air-clad fiber discussed in Section V. Here the air-holes are exploited to directly manipulate the core mode as well as isolate the cladding modes from the central core region and only a single layer of air-holes is required for guidance. Except for an asymmetry caused by the photosensitive core region, this fiber is similar in design to that used in recent experiments by Ranka *et al.* [17], which exploited the small effective area and dispersive properties to generate a visible super continuum. A Bragg grating in the core of this type of fiber will reveal the cladding mode properties as well as the potentially interesting polarization properties resulting from the asymmetric microstructure.

B. High-Delta Fiber Grating Spectra

A length of the fiber was first loaded with deuterium to enhance the photosensitivity of the germanium region and then was exposed using 242 nm through a conventional phase mask with a period of $\Lambda_{\text{mask}} = 1.075$ μm where $\Lambda_{\text{FBG}} = \Lambda_{\text{mask}}/2$. This produced a peak index modulation of $\Delta n \sim 10^{-5}$. The transmission spectrum of the FBG is shown in Fig. 17(a) and (b). Note that the resonant wavelength occurs at approximately 1505 nm. Using the Bragg condition we estimate the effective index of the core mode to be approximately $n_{\text{eff}} \simeq 1.40$, which is well below that of silica. The low effective index of the core mode is due to the strong overlap of the core mode with the closely spaced air-regions, and is indicative of the significant waveguide contribution to the dispersion of this fiber, see [18]. Also note from Fig. 17(a) the absence of cladding mode loss for this range of wavelengths. As we show below, because of the small effective inner cladding diameter of this fiber, the cladding modes are offset significantly from the Bragg resonance.

By adjusting the polarization of the probe light we can interrogate the birefringence of the fiber. Note the appearance in Fig. 17(b), of two strong resonances, spaced by approximately 2.5 nm. This polarization splitting is a result of the strong birefringence of $B \sim 2 \times 10^{-3}$, of the ASM fiber, where contributions arise from the asymmetric stresses in the core and the asymmetry in the geometry. We are able to examine the contribution of these two effects by filling the air-holes with polymer and measuring the birefringence as the polymer–silica index difference is tuned. The geometrical contribution to the polarization splitting will decrease as this index difference decreases, whereas the stress induced contribution should remain unchanged because of the uniform properties of the polymer. Measurements of the polarization splitting upon introduction of an index matched polymer into the air-hole regions showed a decrease in birefringence indicating that both factors are likely to be contributing to the birefringence.

C. High-Delta Fibers Modes

The fiber was initially modeled using BPM where we only considered the central region surrounded by infinite silica cladding [see Fig. 16(b)]. The computed modal spectrum shows a core mode with an effective index of $n_{\text{eff}} \sim 1.405$, in good agreement with the experimental measurements described above, and indicates a second mode of the inner cladding region with an effective index of $n_{\text{eff}} \sim 1.25$. Indeed the difference between the lowest modes of the inner cladding region is $\Delta \sim 10\%$, and is much larger than the core-cladding index step in standard fiber; it exhibits similar modal properties to a step-index fiber with $\Delta \sim 30\%$. Consequently, the corresponding cladding mode spectrum in this fiber is offset from the Bragg resonance by as much as 80 nm, consistent with the measured grating spectra. Further simulations of the entire fiber structure (where the outer glass–air interface was incorporated into the simulation) indicate that the core mode is not the fundamental mode of the fiber, that is there exist cladding modes with energy in the outer cladding region that have propagation constants higher than the core mode. These cladding modes (with $n_{\text{eff}} > n_{\text{core}}$) have negligible spatial overlap with the grating in the central core region and thus are not excited by interaction of core guided light with the grating. Alternatively, grating scattered light is confined within the core region due to total internal reflection off of the inner air–silica boundary.

VII. Conclusion

In summary, we have considered grating resonances in four air–silica microstructured optical fibers with limiting charac-

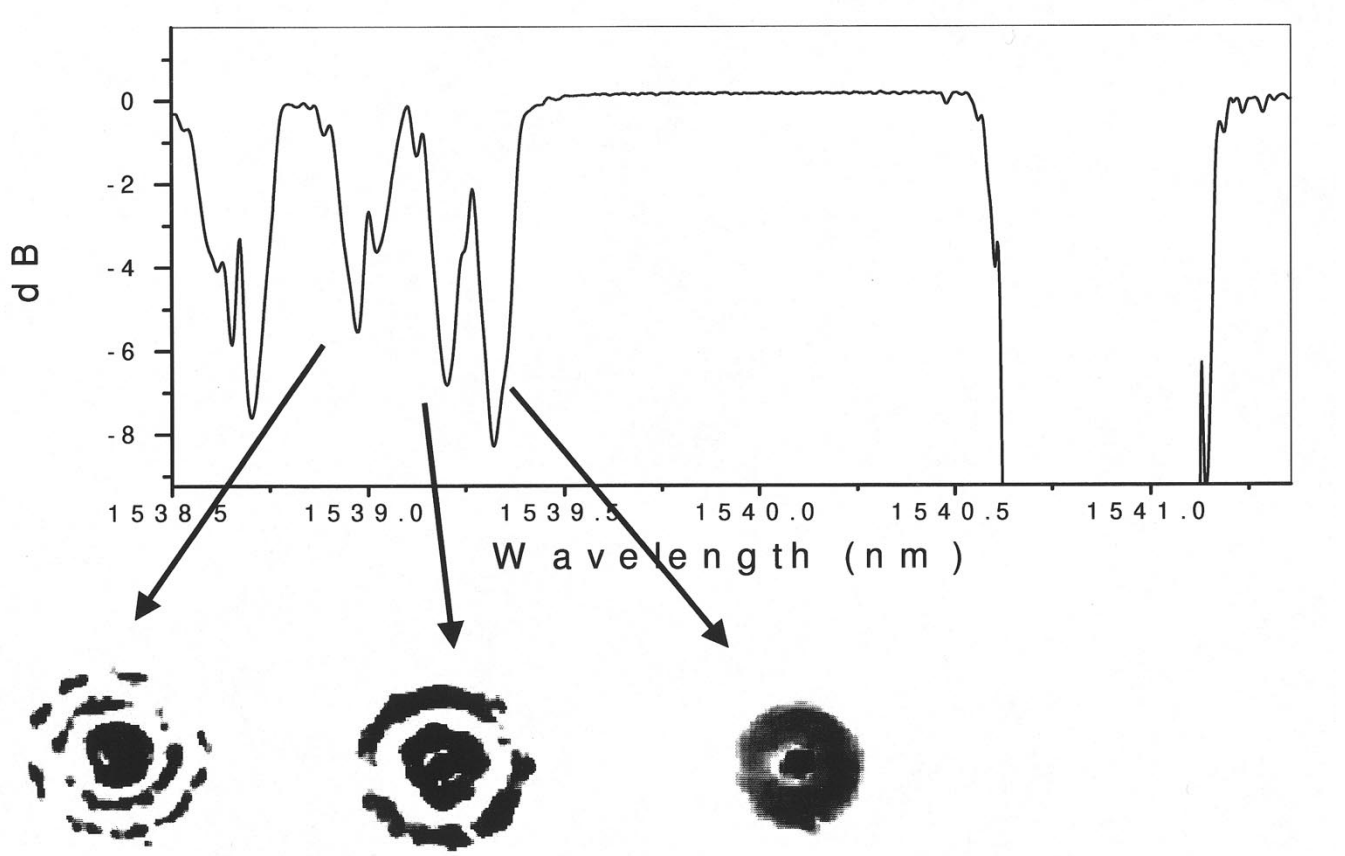

Fig. 15. Near field mode images obtained when the laser wavelength was tuned to: (a) 1539.30 nm (the LP_{02} mode); 1539.20 (LP_{03}); and 1539.00 (LP_{04}).

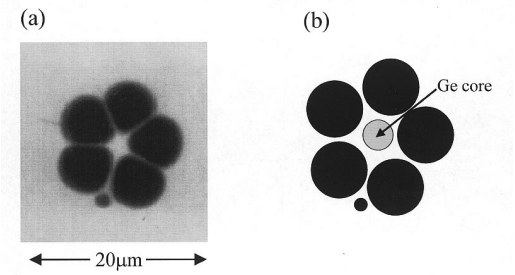

Fig. 16. (a) Shows a photo of the inner region of the high delta microstructured fiber. (b) Schematic.

teristics. By inspection of the transmission spectrum of Bragg gratings written into the core of these fibers we have obtained a knowledge of the guidance properties of light propagating through the air–silica cladding structures, including effective index, "leakiness" or loss due to waveguide structure, and overlap with the core region. The resulting filter characteristics of gratings in these fibers are determined by the characteristics of the microstructure (e.g., fill fraction and/or structure of the array of holes). In particular, the spatial distribution and the effective index of higher order modes can be controlled by the microstructure design. For each fiber type we have demonstrated, by adjusting the details of air-holes, manipulation of core modes and higher order modes that propagate in the cladding, in ways that cannot be achieved in conventional fibers.

The first fiber comprised a core region surrounded by a periodic array of air-holes in the cladding with an air-fill fraction of ~5%. The cladding modes of this fiber are distributed throughout the cladding and are governed by the air-fill fraction. We demonstrated that the cladding modes are leaky, i.e., they penetrate the air-hole barrier and thus are quickly dissipated and exhibit significant bend loss.

The second fiber comprised a core region surrounded by six relatively large air-holes with a corresponding air-fill fraction of ~30%. In this fiber the core mode was unaffected by the air-hole cladding. The lower order cladding modes are confined to the inner silica region and do not extend significantly into the outer cladding region. Higher order cladding modes tunnel through the interstitial regions and thus have some energy in the outer cladding region. As a result, these higher order cladding modes exhibit a small sensitivity to external index. The air-holes create an inner effective cladding with a diameter smaller than that of a conventional fiber, a feature that can be exploited in the design of tunable filters in hybrid air–silica–polymer waveguides formed by infusing polymer into the air regions.

The third fiber comprised an air-ring supported by silica webbing. The cladding modes of this fiber resembled those of conventional fiber and were only slightly perturbed by the webbing region. They also exhibited negligible sensitivity to external index indicating that the cladding modes are confined by the air-ring region.

Finally we considered the high-delta microstructured optical fibers, comprising a central photosensitive core region sur-

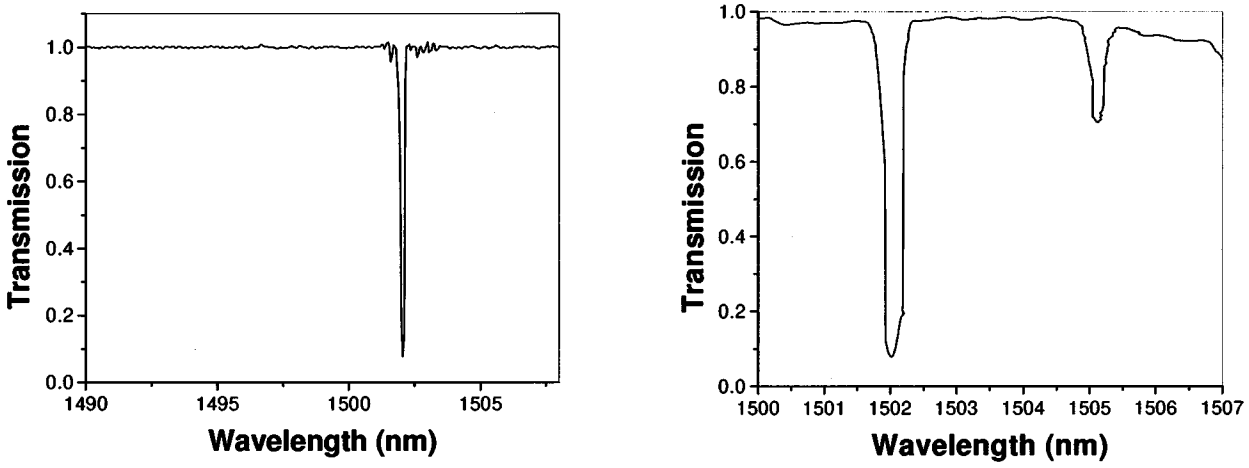

(a) (b)

Fig. 17. (a) Transmission spectra of FBG written into the core of the fiber. (b) Transmission spectra where the launched polarization was adjusted to excited the different principal axis.

rounded by five closely spaced air-holes. Here the air-holes are exploited to manipulate both the core modes and the cladding modes of the fiber. Several observations were made concerning the modal characteristics of this fiber as follows:

a) the effective index of the core mode was substantially below that of the refractive index of silica;
b) the spacing of the inner cladding modes was increased dramatically because of the small inner cladding diameter, resulting in a dramatic offset of the cladding mode loss from the Bragg resonance;
c) cladding modes with energy in the outer region have little spatial overlap with the core region;
d) the birefringence of the fiber was significantly larger than in conventional fiber.

The good agreement between measured grating spectra and simulated modal spectrum indicate that these types of waveguides can be effectively modeled using BPM. In particular we have demonstrated the ability to calculate both higher order modes and leaky modes of these fibers, both, which are difficult to calculate using conventional mode solvers. We demonstrated that our measurements of near-field mode images are well described by beam propagation calculations, which can accurately compute mode indexes and mode distributions. More importantly, we have demonstrated a very simple relationship between the computed modal spectrum and the transmission spectrum of the measured Bragg grating.

By studying gratings in air–silica microstructured optical fibers we hope to realize novel fiber designs offering unique characteristics in the design of grating-based filters. Here the microstructured fiber is used to manipulate cladding mode characteristics in a way that is difficult to achieve in conventional fiber. We have considered several such applications in this paper, including gratings that are insensitive to external index, tunable LPG filters with enhanced sensitivity, and fibers that have dramatically altered cladding mode loss. One topic that we have not considered, which we are currently investigating, is the impact of dispersion in microstructured optical fibers and how it can be used to manipulate grating spectra. It is well known that dispersion can impact grating spectra [43], particularly in the context of LPGs. the impact of the controllable dispersion of microstructured optical fibers on LPG spectra. We expect that further understanding of the relationship between the air–silica microstructure fiber and its transmission spectrum has potential for enabling novel fiber devices.

ACKNOWLEDGMENT

The authors acknowledge valuable conversations with T. Strasser, M. J. Steel, and B. Reed. The authors also thank R. Huff for drawing the optical fibers. C. Kerbage is a student at Columbia University, New York.

REFERENCES

[1] P. Kaiser and H. W. Astle, "Low-loss single-material fibers made from pure fused silica," *Bell Syst. Tech. J.*, vol. 53, pp. 1021–1039, 1974.
[2] T. A. Birks, J. C. Knight, and P. S. J. Russell, "Endlessly single-mode photonic crystal fiber," *Opt. Lett.*, vol. 22, pp. 961–963, 1997.
[3] J. C. Knight, T. A. Birks, R. F. Cregan, P. S. J. Russell, and J.-P. de Sandro, "Photonic crystals as optical fibers-physics and applications," *Optic. Mater.*, vol. 11, pp. 143–151, 1999.
[4] J. C. Knight, T. A. Birks, P. S. J. Russell, and D. M. Atkin, "All-silica single-mode optical fiber with photonic crystal cladding," *Opt. Lett.*, vol. 21, pp. 1547–1549, 1996.
[5] J. Broeng, D. Mogilevstev, S. E. Barkou, and A. Bjarklev, "Photonic crystal fibers: A new class of optical waveguides," *Optic. Fiber Technol.*, vol. 5, pp. 305–330, 1999.
[6] R. S. Windeler, J. L. Wagener, and D. J. DiGiovanni, "Silica–air microstructured fibers: Properties and applications," in *Proc. Optic. Fiber Commun.*, San Diego, CA, 1999, Paper FG1.
[7] T. M. Monro, D. J. Richardson, N. G. R. Broderick, and P. J. Bennet, "Holey optical fibers: An efficient modal model," *J. Lightwave Technol.*, vol. 17, pp. 1093–1102, 1999.
[8] R. F. Cregan, B. J. Mangan, J. C. Knight, T. A. Birks, P. S. J. Russell, P. J. Roberts, and D. C. Allan, "Single-mode photonic bandgap guidance of light in air," *Science*, vol. 285, pp. 1537–1539, 1999.
[9] B. J. Eggleton, P. S. Westbrook, R. S. Windeler, S. Spalter, T. A. Strasser, and G. Burdge, "Grating spectra in air–silica microstructured optical fibers," in *Proc. Optic. Fiber Commun. Conf.*, Baltimore, MD, 2000, Paper ThI2.
[10] B. J. Eggleton, P. S. Westbrook, R. S. Windeler, S. Spalter, and T. A. Strasser, "Grating resonances in air–silica microstructures," *Opt. Lett.*, vol. 24, 1999.

[11] D. Mogilevtsev, T. A. Birks, and P. S. J. Russell, "Group velocity dispersion in photonic crystal fibers," *Opt. Lett.*, vol. 23, pp. 1662–1664, 1998.
[12] T. A. Birks, D. Mogilevtsev, J. C. Knight, and P. S. J. Russell, "Dispersion compensation using single-material fibers," *IEEE Photon. Technol. Lett.*, vol. 11, pp. 674–676, 1999.
[13] R. P. Espindola, R. S. Windeler, A. A. Abramov, B. J. Eggleton, T. A. Strasser, and D. J. D. Giovanni, "External refractive index insensitive air-clad long period fiber grating," *Electron. Lett.*, vol. 35, pp. 327–328, 1999.
[14] A. A. Abramov, B. J. Eggleton, J. A. Rogers, R. P. Espindola, A. Hale, R. S. Windeler, and T. A. Strasser, "Electrically tunable efficient broad-band fiber filter," *IEEE Photon. Technol. Lett.*, vol. 11, pp. 445–447, 1999.
[15] P. S. Westbrook, B. J. Eggleton, R. S. Windeler, A. Hale, T. A. Strasser, and G. Burdge, "Control of waveguide properties in hybrid polymer–silica microstructured optical fiber gratings," in *Proc. Optic. Fiber Commun.*, Baltimore, MD, 2000, Paper ThI3.
[16] ——, "Cladding mode resonances in hybrid polymer–silica microstructured optical fiber gratings," *IEEE Photon. Technol. Lett.*, vol. 12, pp. 495–497, 2000.
[17] J. K. Ranka, R. S. Windeler, and A. J. Stentz, "Efficient visible continuum generation in air–silica micostructured optical fibers with anomalous dispersion at 800 nm," in *Proc. Conf. Laser Electrooptics*, Baltimore, MD, 1999, Postdeadline CPD8.
[18] J. K. Ranka, R. S. Windeler, and A. J. Stentz, "Visible continuum generation in air–silica microstructure optical fibers with anomalous dispersion at 800 nm," *Opt. Lett.*, vol. 25, pp. 25–27, 2000.
[19] J. C. Knight, T. A. Birks, R. F. Cregan, P. S. J. Russell, and J.-P. d. Sandro, "Large mode area photonic crystals," *Electron. Lett.*, vol. 34, pp. 1347–1348, 1998.
[20] T. Erdogan, "Fiber grating spectra," *J. Lightwave Technol.*, vol. 15, pp. 1277–1294, 1997.
[21] ——, "Cladding mode resonances in short- and long-period fiber grating filters," *J. Opt. Soc. Amer. A*, vol. 14, pp. 1760–1773, 1997.
[22] R. Kashyap, *Fiber Bragg Gratings*, 1st ed. New York: Academic, 1999.
[23] A. M. Vengsarkar, P. J. Lemaire, J. B. Judkins, V. Bhatia, T. Erdogan, and J. E. Sipe, "Long-period fiber gratings as band-rejection filters," *J. Lightwave Technol.*, vol. 14, pp. 58–65, 1996.
[24] M. O. Berendt, A. Bjarklev, L. Gruner-Nielsen, and C. E. Soccolich, "Reduction of Bragg grating-induced coupling to cladding modes," *Fiber and Integr. Opt.*, vol. 18, pp. 255–272, 1999.
[25] D. G. Hall, *Theory of Waveguides and Lasers*. New York: Marcel Dekker, 1987.
[26] D. Marcuse, *Theory of Dielectric Optical Waveguides*. New York: Academic, 1991.
[27] M. D. Felt and J. J. A. Fleck, "Computation of mode eigenfunctions in graded index optical fibers by the propagating beam method," *Appl. Opt.*, vol. 19, pp. 2240–2246, 1980.
[28] D. Yevick and W. Bardyszewski, "Correspondance of variational finite-difference (relaxation) and imaginary-distance propagation for modal analysis," *Opt. Lett.*, vol. 17, pp. 329–330, 1992.
[29] R. Scarmozzino, A. Gopinath, R. Pregla, and S. Helfert, "Numerical techniques for modeling guided-wave photonic devices," *IEEE J. Select. Topics Quantum Electron.*, vol. 6, pp. 150–162, 2000.
[30] J. Martin and F. Ouellette, "Novel writing techniques of long in-fiber gratings," *Electron. Lett.*, vol. 30, pp. 811–812, 1993.
[31] T. A. Strasser, P. J. Chandonnet, J. DeMarko, C. E. Soccolich, J. R. Pedrazzani, D. J. Digiovanni, M. J. Andrejco, and D. S. Shenk, *Optic. Fiber Commun.*, 1996.
[32] J. C. Knight, T. A. Birks, P. S. J. Russell, and J. P. d. Sandro, "Properties of photonic crystal fiber and the effective index model," *J. Opt. Soc. Amer. A*, vol. 15, pp. 748–752, 1998.
[33] D. R. Scarmozzino, *BeamPROP*, 3rd ed. New York: Rsoft Inc., 1999.
[34] D. B. Stegall and T. Erdogan, "Leaky cladding mode propagation in long-period fiber grating devices," *IEEE Photon. Technol. Lett.*, vol. 11, pp. 343–345, 1999.
[35] L. Dong, L. Reekie, and J. L. Cruz, "Long period gratings formed in depressed cladding fibers," *Electron. Lett.*, vol. 33, pp. 1897–1899, 1997.
[36] S. J. Hewlett, J. D. Love, G. Meltz, T. J. Bailey, and W. W. Morey, "Coupling to photo-induced Bragg gratings in depressed- and matched cladding fiber," *Optic. Quantum Electron.*, vol. 28, pp. 1641–1654, 1996.
[37] B. H. Lee, Y. Liu, S. B. Lee, S. S. Choi, and J. N. Jang, "Displacement of the resonant peaks of a long-period fiber grating induced by a change of ambient refractive index," *Opt. Lett.*, vol. 22, pp. 1769–1771, 1997.
[38] B. J. Eggleton, J. A. Rogers, P. B. Westbrook, and T. A. Strasser, "Electrically tunable power efficient dispersion compensating fiber Bragg grating," *IEEE Photon. Technol. Lett.*, vol. 11, pp. 854–856, 1999.
[39] B. J. Eggleton, J. A. Rogers, P. S. Westbrook, G. Burdge, S. Ramachandran, A. A. Abramov, T. N. Nielsen, G. R. Kowach, R. S. Windeler, and T. A. Strasser, "Tunable fiber grating devices utilizing integrated thin film heaters," in *WDM Components*, D. A. Nolan, Ed. Washington, DC: Opt. Soc. Amer., 1999, pp. 61–72.
[40] J. A. Rogers, B. J. Eggleton, and P. Kuo, "Temperature stabilized operation of tunable fiber grating devices that use distributed on-fiber thin film heaters," *Electron. Lett.*, vol. 35, pp. 2052–2053, 1999.
[41] H. J. Patrick, A. D. Kersey, and F. Bucholtz, "Analysis of the response of long-period gratings to external index of refraction," *J. Lightwave Technol.*, vol. 16, pp. 1606–1612, 1998.
[42] A. Abramov, A. Hale, R. S. Windeler, and T. A. Strasser, "Broadly tunable long-period fiber grating filter," *Electron. Lett.*, 1999.
[43] T. Erdogan and D. Stegall, "Impact of dispersion on the bandwidth of long-period fiber grating filters," in *Proc. Optic. Fiber Commun.*, Dallas, TX, 1998.

B. J. Eggleton received the Bachelor degree with Honors in physics from the University of Sydney, Sydney, New South Wales, Australia. He received the Ph.D. degree from the School of Physics and the Optical Fiber Technology Center in the Australian Photonics Cooperative Research Center, at the University of Sydney, in 1996. His doctoral research focused on linear and nonlinear effects in fiber gratings. The highlight of this research involved the first observation of nonlinear propagation effects in photonic bandgap structures for which he was awarded the 1998 Adolph Lomb Medal from the Optical Society of America.

From November 1996 to June 1998, he was a Postdoctoral Member of Technical Staff in the department of Optical Physics at Bell Laboratories, Lucent Technologies, Murray Hill, NJ. In July 1998, he joined the Optical Fiber Research Department at Bell Laboratories, as a Member of Technical Staff. His research interests include nonlinear optics, Bragg soliton phenomena, fiber optics, fiber gratings, photonic bandgap structures, air-silica microstructured optical fibers, all-optical switching devices and dispersion compensation techniques in WDM lightwaves systems.

P. S. Westbrook received the Ph.D. degree in physics from Massachusetts Institute of Technology, Cambridge, in 1998.

He joined the staff of Bell Labs in 1998 as a Postdoctoral in the fiber devices research area. He is currently a Member of Technical Staff at Bell Labs in the area of fiber waveguide research and has worked on several topics including in-fiber polarization monitoring and control, hybrid polymer-silica fibers, air-silica microstructure fibers, and dispersion compensating fiber gratings.

C. A. White received the B.S. degree in chemistry from Carnegie Mellon University, Pittsburgh, PA, in 1992 and the Ph.D. degree in theoretical chemistry from the University of California, Berkeley in 1997. His thesis work concerned the development of numerical methods for the treatment of proteins and other large molecular systems.

In September 1997, he joined Lucent Technologies, Bell Laboratories as a Member of Technical Staff in the Materials Chemistry Research Department. His current research interests concern the development of new computational methods for simulating the behavior of optical systems.

C. Kerbage received the B.Sc. degree in physics from the American University of Beirut, the M.S. degree in applied physics from Columbia University, New York. He is now pursuing the Ph.D. degree in optical physics at the Department of Applied Physics at Columbia University.

He is engaged in research and development of optical fibers at Bell Laboratories, Lucent Technologies in the Optical Fiber Research Department.

R. S. Windeler received the B.S. degree in chemical engineering from the University of Delaware, Newark, in 1990, and the M.S. and Ph.D. degrees in chemical engineering from the University of California, Los Angeles in 1992 and 1995, respectively.

He became a Member of Technical Staff at Bell Laboratories, Lucent Technologies in 1995 and is a member of the Optical Fiber Research Department where he has extensive experience in fiber fabrication and design. His areas of expertise include MCVD, modified MCVD, and solution doping which he has used to produce world class specialty fibers. His current research efforts involve fabrication and design of Er-Yb double-clad fiber for high power amplifiers and microstructured air-silica fibers. His microstructured fibers were used to demonstrate for the first time anomalous dispersion below 1290 nm, zero group-velocity dispersion as low as 765 nm, and many nonlinear interactions in the near visible region including soliton propagation, self phase modulation, pulse compression, and ultra broadband continuum generation. He holds two patents and has over ten pending patents on production and use of optical fiber.

G. L. Burdge, photograph and biography not available at the time of publication.